Anal. Chem. **2009,** *81,* 1365–1370

Integration of Low-Power Microfluidic Pumps with Biosensors within a Laboratory-on-a-Chip Device

Gerald Blanco-Gomez,[†] Andrew Glidle,[†] Leonard M. Flendrig,[‡] and Jon M. Cooper*,[†]

Department of Electronics and Electrical Engineering, University of Glasgow, Glasgow G12 8LT, U.K., and Unilever R&D Vlaardingen, Dept. FSD, Vlaardingen 3130AC, Netherlands

We describe the fabrication of a controllable microfluidic valve coupled with an electrochemical pump, which has been designed to deliver reagents to an integrated microfluidic biosensing system. Fluid, retained within an insertion reservoir using a stop valve, was pumped using electrochemical actuation, providing a low power, low voltage integrated Laboratory-on-a-Chip for reproducible, small volume fluidic manipulation. The properties of the valve were characterized using both X-ray photoelectron spectroscopy and contact angle measurements, enabling the calculation of the magnitude of the forces involved (which were subsequently verified through experimental measurement). Electrochemical generation of oxygen and hydrogen acted as an on-demand pressure system to force fluid over the stop valve barrier. The process of filling-up the biosensing chamber was characterized in terms of the time to fill, the energy used, and the peak power consumed. The potential of the device was illustrated using a glucose biosensor.

It is anticipated that autonomous microfluidic biological sensing systems will find diverse applications in a variety of remote sensing opportunities, including those for astrobiology, ecological measurements under the sea or in the arctic,[1] or within the medical field, in Laboratory-on-a-pill[2] formats for in situ gastro-intestinal monitoring or intra-ocular drug delivery.[3] In such devices, it will be necessary to implement low voltage-low power actuation of fluid flow, to enable simple analytical protocols. In situ microfluidic pumping will enable a series of analytical proposals, including reagent delivery and sensor calibration. In more advanced biosensing systems, based, for example, on heterogeneous immunoassays such as the ELISA, the technology may also prove important in the implementation of one or more separation steps (e.g., in the removal of unbound, labeled antibodies in a heterogeneous immunosensor).

Here, we report on an integrated valve, sensor, and pump to enable a model analytical measurement, based upon the implementation of a glucose microbiosensor. The valve was comprised of a photolithographically patterned hydrophobic barrier[4,5] in a microfluidic channel that controlled the flow of analyte, leading to an electrochemical detection sensor system. The microfluidic pumping unit was enabled through the local electrolysis of water to generate hydrogen and oxygen gas, and so provide the pressure driven flow[6−14] necessary to overcome the hydrophobic barrier, according to the following reactions:

$$2H_2O + 2e^- \leftrightarrow H_2 + 2OH^- \qquad \text{at} - 0.83 \text{ V versus Normal Hydrogen Electrode (NHE) at 298 K}$$

$$O_2 + 4e^- + 4H^+ \leftrightarrow 2H_2O \qquad \text{at 1.23 V versus NHE at 298 K}$$

The relation between the gas volume generated (creating pressure driven flow) and the charge passed was expressed as $V_{H_2} = V_m Q/2F$, $V_{O_2} = V_m Q/4F$, where F is the Faraday constant, Q is the charge passed through the electrodes, and V_m is standard molar volume.

The future potential applications of such integrated sensory devices provide constraints on both the valve and the pump. For example, we considered the need for a passive valve, whose mechanism could be electronically triggered by the user (e.g., by a wireless signal). A second design constraint was that the whole system should operate under low voltages (4 V) and power (5 mW). This second point, coupled with our aim that the overall size of the device should be as small as possible, as would be the

* To whom correspondence should be addressed. E-mail: j.cooper@elec.gla.ac.uk.

[†] University of Glasgow.

[‡] Unilever R&D Vlaardingen.

(1) Wilson, R.; Monaghan, P.; Bowden, S. A.; Parnell, J.; Cooper, J. M. *Anal. Chem.* **2007**, *79*, 7036–7041.

(2) Johannessen, E. A.; Wang, L.; Reid, S. W. J.; Cumming, D. R. S.; Cooper, J. M. *Lab Chip* **2006**, *6*, 39–45.

(3) Lo, R.; Li, P. Y.; Saati, S.; Agrawal, R.; Humayun, M. S.; Meng, E. *Lab Chip* **2008**, *8*, 1027–1030.

(4) Lee, S. H.; Lee, C. S.; Kim, B. G.; Kim, Y. K. *J. Micromech. Microeng.* **2003**, *13*, 89–97.

(5) Handique, K.; Burke, D. T.; Mastrangelo, C. H.; Burns, M. A. *Anal. Chem.* **2000**, *72*, 4100–4109.

(6) Bohm, S.; Timmer, B.; Olthuis, W.; Bergveld, P. *J. Micromech. Microeng.* **2000**, *10*, 498–504.

(7) Neagu, C. R.; Gardeniers, J. G. E.; Elwenspoek, M.; Kelly, J. J. *J. Microelectromech. Syst.* **1996**, *5*, 2–9.

(8) Tas, N. R.; Berenschot, J. W.; Lammerink, T. S. J.; Elwenspoek, M.; van den Berg, A. *Anal. Chem.* **2002**, *74*, 2224–2227.

(9) Pal, R.; Yang, M.; Johnson, B. N.; Burke, D. T.; Burns, M. A. *Anal. Chem.* **2004**, *76*, 3740–3748.

(10) Xie, J.; Miao, Y. N.; Shih, J.; He, Q.; Liu, J.; Tai, Y. C.; Lee, T. D. *Anal. Chem.* **2004**, *76*, 3756–3763.

(11) Furdui, V. I.; Kariuki, J. K.; Harrison, D. J. *J. Micromech. Microeng.* **2003**, *13*, S164−S170.

(12) Cameron, C. G.; Freund, M. S. *Proc. Natl. Acad. Sci. U.S.A.* **2002**, *99*, 7827–7831.

(13) Fuentes, H. V.; Woolley, A. T. *Lab Chip* **2007**, *7*, 1524–1531.

(14) Hua, S. Z.; Sachs, F.; Yang, D. X.; Chopra, H. D. *Anal. Chem.* **2002**, *74*, 6392–6396.

10.1021/ac802006d CCC: $40.75
Published on Web 01/14/2009

Scheme 1. (A) Schematic of the Device Top View Showing the Complete System, [a] (B) Microfluidic Channel (Side View) Containing the Stop Valve, and [b] (C) Three Phases (Liquid, Solid, Gas) Contact Line Interface with Their Associated Surface Tension Considered for a Droplet of Water Deposited on a Solid Surface in Air

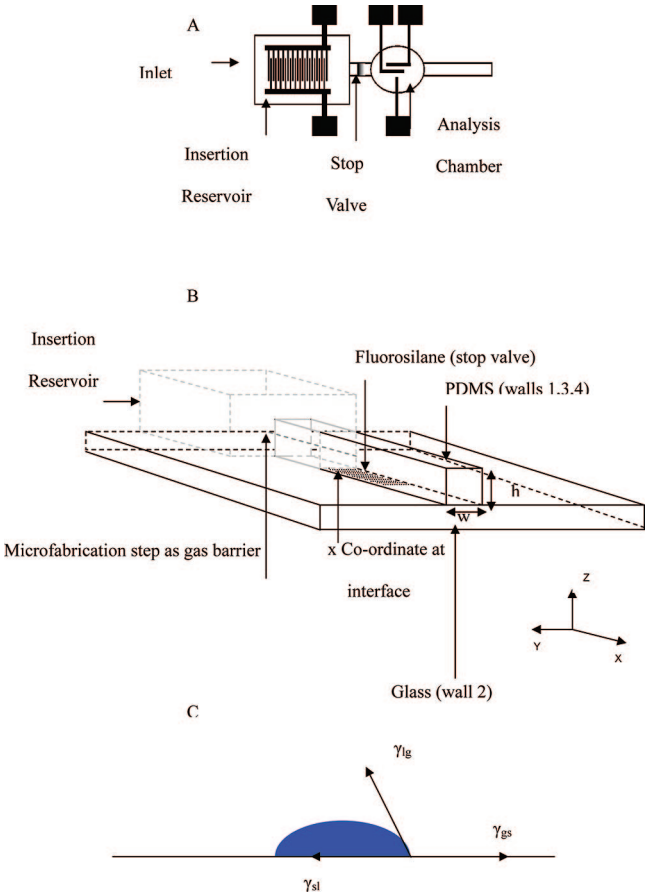

[a] The storage reservoir containing interdigitated electrodes was 3.5 mm in length, the channel containing the stop valve was 1 mm long, and the sensing chamber 2.5 mm in length, giving the whole device a size of ~0.7 cm. [b] The distance reached by the liquid slug before being retained by the microfluidic barrier is marked as ×; (b) also shows the barrier in the channel to prevent the gas from moving into the analytical chamber. The gray dashed lines represent the microfluidic region were liquid can spread until being stopped by the valve, acting also as a barrier to the movement of electrogenerated gas bubbles. Walls 1, 3, 4 are the top and sides walls, made of PDMS, while wall 2 (the base) was made of glass.

case in Laboratory-on-a-Pill, prevented the use of many off-the-shelf components (including pressure driven MEMS pumps, for example).

In this paper, we describe the design of the valve, which was integral to the functioning of the microsystem. We subsequently describe its fabrication and demonstrate the storage and pumping of reagents to the biosensor interface (e.g., for calibrating a sensor).

BACKGROUND

System Overview. The device was fabricated as two subsystems, the first of which comprised the patterning of electrochemical actuators (interdigitated electrodes for pressure driven pumping), biosensors (as a three electrode cell, for glucose detection), and a stop valve. These components were all defined by photolithography, metal evaporation, and lift off on a glass or silicon substrate.

The second subsystem involved the creation of an insertion reservoir for the storage of the reagents, microfluidic channels, and the definition of the sensing chamber using the polymer, poly(dimethylsiloxane), PDMS. A schematic of the complete system is shown in panels a and b of Scheme 1.

Theory. At the micrometer scale, the Bond number[15] tells us that interfacial forces will dominate over viscous and gravitational forces. For example, when considering a standard PDMS channel, sealed against a glass slide (with three sides of PDMS (walls 1, 3, and 4) and a base plate of glass (wall 2) with dimensions of w (width), h (height), and L (length)), Scheme 1B, filled with an aqueous liquid, the Bond number is well below unity ($\sim 10^{-3}$). To fully understand the forces acting within such a fluidic channel, a number of assumptions are made both in the context of the pressures and forces (relating to two different channel surface tensions associated with PDMS and glass), and a triple phase boundary (as a result of the interface between the gas, liquid and either glass or PDMS), Scheme 1C.

Given these assumptions, any microfluidic actuation, operating under the action of the three forces in the channel can be expressed by quantifying the total internal energy, using eq 1:[16]

$$E = \sum_{i=1}^{N} (A_{\mathrm{lg}i}\gamma_{\mathrm{lg}i} + A_{\mathrm{sg}i}\gamma_{\mathrm{sg}i} + A_{\mathrm{sl}i}\gamma_{\mathrm{sl}i}) \quad (1)$$

where N is an integer, representing the number of different liquid−gas−solid interfaces considered within the structure; i is also an integer and takes value in the range [1, N], $A_{\mathrm{lg}i}$, $A_{\mathrm{sg}i}$, $A_{\mathrm{sl}i}$, are the areas of interface between liquid−gas (lg$i$), solid−gas (sg$i$) and solid−liquid (sl$i$) respectively; and $\gamma_{\mathrm{lg}i}$, $\gamma_{\mathrm{sg}i}$, and $\gamma_{\mathrm{sl}i}$ are the associated surface tensions per unit area, Scheme 1C. A liquid inside such a microfluidic channel can therefore be considered as having four interface dependent contact angles one for each wall (where the contact angle depends on the properties of the channel wall, with the fluid phases being assumed to be air and water).

Using the Cartesian reference axes, Scheme 1B, fluid motion was considered in the x-axis with the triple phase interface referenced to an x coordinate. This led to the following expression for the internal energy, considering the four-walled channel, as described:

$$E = (L - x)[w(\gamma_{\mathrm{sg1}} + \gamma_{\mathrm{sg2}}) + h(\gamma_{\mathrm{sg3}} + \gamma_{\mathrm{sg4}})] + x[w(\gamma_{\mathrm{sl1}} + \gamma_{\mathrm{sl2}}) + h(\gamma_{\mathrm{sl3}} + \gamma_{\mathrm{sl4}})] + \sum_{i=1}^{n} A_{\mathrm{lg}i}\gamma_{\mathrm{lg}i} \quad (2)$$

By using Laplace's law and differentiating eq 2 with respect to the flow (along the x-axis), and combining this with the steady-state case of Young's law, provides an estimate for the interfacial pressure difference, ΔP, along x, as $-\delta E/\delta V$, with δV being the volume of fluid displaced.

(15) Gunther, A.; Jensen, K. F. *Lab Chip* **2006**, *6*, 1487–1503.
(16) Feng, Y.; Zhou, Z.; Ye, X.; Xiong, J. *Sens. Actuators, A* **2003**, *108*, 138–143.

Thus, for a channel of molded PDMS, sealed against a glass substrate (as used in this paper), with channel walls 1, 3, and 4 having a PDMS−water−air interface (see Scheme 1B) with equal contact angles, θ_1, θ_3, and θ_4 and channel wall 2 having a glass−water−air interface with a different contact angle θ_2, we can write an expression for a pressure difference, ΔP, at the interface accordingly:

$$\Delta P = \gamma_{lg}\left[\frac{(w+2h)}{wh}(\cos\theta_1) + \frac{w}{wh}(\cos\theta_2)\right] \quad (3)$$

where γ_{lg} is the liquid−gas (water−air) surface tension per unit area (as $\gamma_{lg1} = \gamma_{lg2}$). This equation is similar to that previously described in the literature, although the pressures and directions of flow differ.[16−18]

To illustrate eq 3, we can calculate the value of the pressures within a 20 μm high, 400 μm wide channel by measuring the water−PDMS contact angle (θ_1), measured as 110° (Drop Shape Analysis System, Easy Drop, Kruss GmbH, Germany) and the water−glass contact angle (θ_2) measured as 40°. Given the surface tension of water in air as 72.75 mN m^{-1}, we estimate a forward pressure of 1.42 kPa, which would exist, thereby moving the solution along the channel.

By modifying the glass surface using a silane based chemistry, and changing the contact angle of θ_2 from 40° to 115°, we can estimate that a back-pressure of 2.88 kPa could be generated. This would retain the fluid behind the modified area. This provides an estimate of the forces opposing flow when a valve is created using a photolithographically patterned hydrophobic silane.

Lastly, considering an incompressible fluid under a constant flow and with no effect from gravity, the Navier−Stokes equation allows us to relate pressure difference in a channel with the liquid flow rate. If we also assume that the channel width is greater that the channel height, we can consider a Poiseuille flow ruled by the infinite parallel-plate condition, expressed as eq 4:[19]

$$P_{PF} = \frac{12\mu LQ}{h^3 w} \quad (4)$$

where μ is the dynamic viscosity, Q is the flow rate, and P_{PF} is the pressure difference between the extremities of the fluid plug in the channel section ($w \times h$).

MATERIALS AND METHODS

As stated, the device was assembled as two subsystems, involving three separate fabrication processes, namely, the patterning of microelectrodes (both for sensing and for pressure driven flow actuation); the deposition of fluorosilane to create a stop valve; and the replica molding of microfluidic channels in PDMS against an photolithographically patterned SU-8 master.

Patterning Microelectrodes. Immediately prior to microelectrode fabrication, 0.8 mm thick glass substrates were cleaned, and a wet etch was performed using HF to create a recess of 250 ± 10 nm into which the electrodes will be deposited (so the PDMS channel will seal against a flat surface). To achieve this, substrates were first cleaned and spin-coated with S1818 (Shipley, U.K.) photoresist. Pattern transfer resulted in the creation of a photoresist mask for a standard HF-glass wet etch. Alignment features were also patterned into the glass to enable the electrodes to be registered into the recess.

A second photolithographic procedure was then used to define the pump and sensor microelectrodes into a second layer of spin coated S1818. Microelectrodes, comprising a 20 nm Ti adhesion layer and a 125 nm Pt top layer were deposited using metal evaporation and lift-off.

Fluorosilane Deposition. A third coating of S1818 resist was then spun on the substrate, and the stop-valve pattern similarly defined, using pattern transfer, silanization, and lift-off. Following exposure and development of the resist, the surface was cleaned using an oxygen barrel asher at 100 W, for 2 min, immediately before surface modification. The exposed area was modified with 1.5 mM 1*H*,1*H*,2*H*,2*H*-perfluorooctyl-trichlorosilane, FOTS, in heptane for 2 min, to change the contact angle.[5,20−22]

Fluidic Network. Finally, a microfluidic network created using PDMS replica molding[23] against an SU-8 patterned master was aligned to the pattern of electrodes and the stop valve on the glass substrate and was sealed by pressure bonding. Importantly, a physical step in the channel height between the electrolysis and the analysis chambers was incorporated into the microfluidic channel design to act as a physical barrier, preventing bubbles (created during electrolysis) from entering the analysis chamber, see Scheme 1 b.

Surface Characterization. Analysis was performed using both contact angle measurements at 22 °C and X-ray photoelectron spectroscopy to validate the nature of the FOTS coating used for the stop valve. XPS spectra were collected using a Scienta ESCA300 (XPS, 8 kW Al K(α) and Cr K(β) dual source, 1487 eV energy) performed at the National Centre for Electron Spectroscopy and Surface Analysis, Daresbury Laboratory, U.K. The energy resolution was 0.025 eV, and the spatial resolution used to map a FOTS pattern was 25 μm.

Both the unmodified glass substrate, which had undergone a simple cleaning, and a glass substrate modified with FOTS were analyzed. An electron take off angle (TOA) of 45° was used, and recordings were carried out with a pass energy of 75 eV and a window pass energy of 20 eV. Spectra were collected for the following orbitals: C(1s), O(1s), N(1s), Si(2p), F(1s), Na(1s), Mg(1s). Data collection and processing from XPS experiments were performed with the software ESCA Analysis. Using linear backgrounds, as well as standard orbital sensitivity factors for each element, a quantification table was compiled for both samples.

Assessment of Valve Operation. The device inlet was connected to a three-way valve, switching between the chip, a microliter precision glass pipet, and a water column, using standard PTFE interconnects. The chip was first filled manually using the precision pipet. Using an optical microscope, it was noted that fluid filled the channel up to the FOTS coated on-chip valve.

(17) Andersson, H.; Van der Wijngaart, W.; Griss, P.; Niklaus, F.; Stemme, G. *Sens. Actuators, B* **2001**, *75*, 136–141.
(18) Kim, E.; Whitesides, G. M. *J. Phys. Chem. B* **1997**, *101*, 855–863.
(19) Bruus, H. *Theoretical microfluidics*; Oxford University Press: New York, 2008.
(20) Ochsner, M.; Dusseiller, M. R.; Grandin, H. M.; Luna-Morris, S.; Textor, M.; Vogel, V.; Smith, M. L. *Lab Chip* **2007**, *7*, 1074–1077.
(21) Zhao, B.; Moore, J. S.; Beebe, D. J. *Science* **2001**, *291*, 1023–1026.
(22) Brzoska, J. B.; Benazouz, I.; Rondelez, F. *Langmuir* **1994**, *10*, 4367–4373.
(23) Xia, Y. N.; Whitesides, G. M. *Annu. Rev. Mater. Sci.* **1998**, *28*, 153–184.

A column of fluid was then connected "in-line" to the chip, and its height was gradually raised until the valve "burst" was observed.

Biosensor Fabrication. A three-electrode glucose biosensor was fabricated in the analytical microchamber, described above. The working and counter electrode had both an area of ~0.3 mm^2. The reference electrode was made from Pt and acted as a pseudo reference. The three electrodes were first cleaned with acetone and IPA before soaking in a H_2SO_4/H_2O_2 solution for 5 min. The electrodes were then washed in RO water. Poly(pyrrole) was codeposited with the enzyme glucose oxidase (GOD) on the working electrode. The process first involved the absorption of GOD onto the working electrode for 1 h from a solution of 220 units/mL enzyme in 50 mM potassium phosphate buffer, pH 7.2, containing 50 mM KCl. Following this, GOD was copolymerised on the working electrode from a solution containing 1 mg/mL enzyme and 30 mM pyrrole in a supporting electrolyte of 50 mM potassium phosphate buffer, pH 7.2 containing 50 mM KCl. The potential at the working electrode was scanned between 0.1 V and 0.9 V at 50 mV/s using an external platinum electrode as a combined pseudo-reference and counter electrodes (note that the absolute value of the voltage has less analytical significance as a pseudo-reference was being used). After 10 scans, the electrodes were rinsed thoroughly with buffer, to remove non-specifically absorbed enzyme.

Fluid Pumping. The device was assembled and the reservoir was loaded by capillary forces following the placement of a ~0.8 μL droplet of calibration solution at the inlet (Scheme 1a), at which point the device inlet was sealed. Experiments were carried out using 50 mM potassium phosphate buffer, pH 7.2, containing 50 mM NaCl and 0.5 mg/mL pluronic F127. Standard additions of glucose (up to 25 mM) were used, as required. Electrolysis was performed using a CV-37 potentiostat (BAS Instruments Ltd., Cheshire, U.K.).

Biosensor Analysis. Prior to the measurement, the background current was measured at an electrochemical potential of 0.0 V to check the reliability of the pseudo-reference electrode. Solutions containing 0.25 mM, 1.8 mM, 8.3 mM, 13.6 mM, 23.2 mM glucose in phosphate buffer containing supporting electrolyte were flowed onto the electrodes, and the steady state current was measured, providing a proof-of-concept for sensor calibration.

RESULTS AND DISCUSSION

Surface Characterization. Contact angles were measured as 110 ± 2° and 115 ± 2° for different sized droplets on PDMS and FOTS modified glass surfaces, respectively. Using channel dimensions of 400 μm wide and 20 μm high and eq 3, we estimated that the static back-pressure difference at the interface will be about 3 kPa, sufficient to constrain fluid flow within the insertion reservoir. Under these circumstances, the hydrophobic barrier acts as a valve, stopping the flow of water.

The fluorosilanization process was further characterized by patterning FOTS and collecting XPS spectra. A clean, unmodified glass substrate was compared with a glass substrate modified with FOTS, as described above. Assuming linear backgrounds, as well as standard orbital sensitivity factors for each element, it was possible to compare the composition of the unmodified (C(1s) (8%), O(1s) (40%), Si(2p) (37%), Na(1s) (5%), F(1s) (2%)) and the

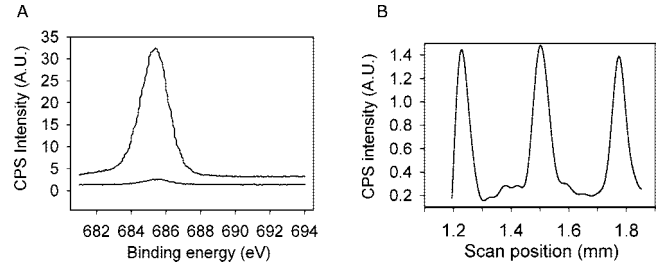

Figure 1. Left (A) panel shows the F(1s) spectra for glass (solid line) and glass/FOTS (dotted line). Curves display the number of counts collected per second as a function of binding energy in eV (offset due to the use of the flood gun). Curves were fitted with the software ESCA Analyses; right (B) panel shows a 1D spatial position-binding energy XPS image (not shown) from a stripe patterned fluorosilane modified sample. After integration of the counts under the F(1s) peaks, a graph of spatial position versus integrated F(1s) counts was obtained for part of this region (three peaks, associated with each of the stripes are shown).

FOTS modified surfaces (C(1s) (17%), O(1s) (36%), Si(2p) (14%), F(1s) (33%)). Significantly, it was noted that the greatly increased amounts of carbon and fluorine on the modified surface, Figure 1 a, coupled with a subsequent reduction in the amount of silicon were consistent with the formation of an FOTS layer (the SiO_2 of the untreated surface, has been covered by the fluorosilane layer).

The ability to photopattern the fluorosilane was also analyzed using 50 μm wide bands of FOTS. XPS maps were collected from an area of 3 mm × 3 mm with a CCD pixel size of 3.2 μm. After processing the data, a graph of spatial position (along one axis of the sample) against F(1s) counts was obtained (Figure 1b). Ultimately, the spatial resolution of the images (ca. 25 μm) was limited by the XPS instrument's optics. The data show that the positive photoresist inhibits penetration by the FOTS-heptane solution, enabling the patterning of a hydrophobic valve.

Valve Back Pressure. Using a hydrostatic method, it was found that the valve burst when the column was raised 27.0 cm (mean, $n = 3$), which can be related to a barometric pressure of 2.65 kPa. This compared to the numerical estimation of pressure (P) from eq 3 of 2.88 kPa (indicating a difference between the numerical estimation and the experimental measurement of ca. 8%).

Fluid Pumping. Following electrolysis for specific periods of time (dependent on the applied voltage, Table 1), electrolytic gas generation created sufficient pressure to overcome the stop valve, with a fixed volume of solution being pumped from the storage reservoir, Scheme 1a, to the analysis chamber. It was found that pumping was only effective when a constant voltage between 3.5 and 4 V was applied across the electrode pair in the insertion chamber. The sequence of bubble formation and fluid flow following electrolysis is as seen in the panels a−d of Figure 2. For each voltage at which the fluid could pass the stop valve, the time required to fill the analysis chamber (actuation time) and electrical power are shown in panels a and b of Figures 3, and tabulated in Table 1. The energy required to dispense a given volume was calculated and shown, together with the rate of fluid flow, in Table 1 for selected voltages. The flow rate was measured during the filling-up process using video imaging (20 ms per frame). The energy to complete the flow was estimated by integrating the actuation current (delivered by interdigitated electrodes) as a function

Table 1. Actuation Parameters and Electric Characteristics for Pressure Driven Flow under Electrolysis at Voltages between 3.5 V and 4.0V[a]

voltage (v)	energy required to inject a unit volume (10^{-11} J μm^{-3})	actuation period (s)	average flow rate observed (μL min^{-1})	estimated Poiseuille pressure after valve break (Pa)	charge (mC)	energy (mJ)	peak power consumption (mW)
3.5	8.4	2.2	1.3	10	1.2	4.2	2.4
3.6	7.5	1.6	1.9	16	1.0	3.7	3.0
3.7	6.7	1.2	2.4	41	0.9	3.3	3.6
3.8	8.1	1.2	2.4	62	1.1	4.1	4.3
3.9	6.8	0.8	3.7	123	0.9	3.4	5.0
4.0	5.9	0.6	4.7	200	0.7	3.0	5.8

[a] The actuation period was considered between the first bubble appearance and the liquid plug reaching the outlet channel.

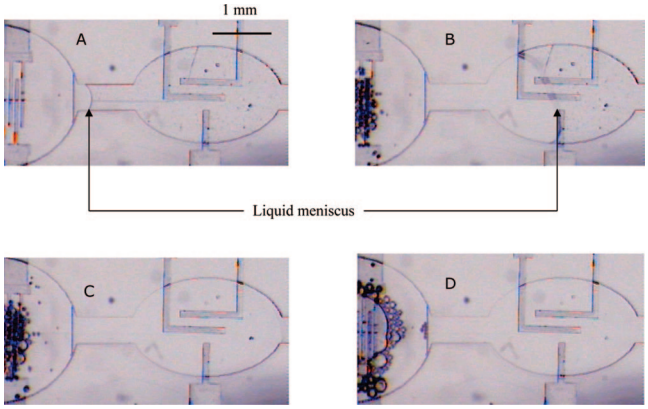

Figure 2. FOTS-based patterned microfluidic valve operation by an integrated electrochemical fluidic actuator. A solution of 50 mM potassium phosphate buffer, pH 7.2 containing supporting electrolyte, was first introduced in the inlet reservoir. Gas bubbles were generated using electrolysis to create pressure driven flow. A series of four pictures (with inverted colors, for clarity) from video acquired during the procedure are as follows: (A) insertion before application of 3.6 V electrolysis; (B) after 0.6 s after electrolysis; (C) after 1.5 s electrolysis; (D) after 5 s, when the analysis chamber was filled. A physical step change in the channel height acts as a barrier to bubbles, preventing their ingress into the analysis chamber.

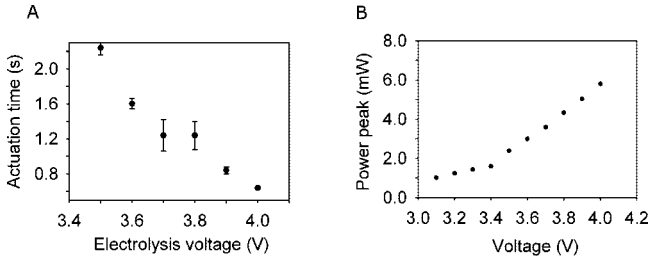

Figure 3. Left panel (A) shows the duration of actuation process which was plotted against the electrolysis voltages (mean and S.E., $n = 3$); and right panel (B) shows peak power as a function of voltage over a 2.5 s electrolysis period.

of time. The energy efficiency was given as the ratio between the actuation energy and the flow rate, measured in J μm^{-3}. Charge, peak power consumption, as well as energy efficiency and flow rate, are displayed in the Table 1.

The maximum efficiency ratio, as well as average flow rate, were both also calculated by considering that only the ~50 nL analysis chamber needs to be filled during electrolysis process. The amount of gas produced during electrolysis below 3.4 V was too low to reproducibly overcome the stop-valve back-pressure. However, at applied voltages above 3.5 V, it was possible to fill

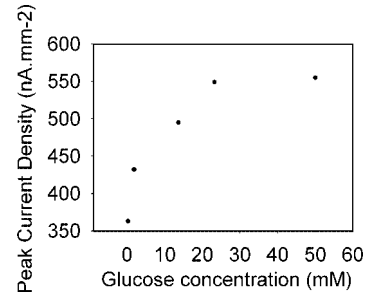

Figure 4. Plot showing peak oxidation currents against glucose concentration for a simple glucose biosensor. The device was based upon the glucose oxidase mediated catalytic production of hydrogen peroxide in the presence of oxygen. The enzyme was immobilized within a poly(pyrrole) conducting polymer film, and hydrogen peroxide was detected amperometrically at a potential of 0.85 V versus a Pt-pseudo reference electrode. Peak oxidation current peaks were found to increase linearly ($r^2 = 0.99$) with glucose concentration between 1.8 mM and 23.2 mM.

the chamber in less than 2.5 s (Table 1). Table 1 also shows the Poiseuille pressure (generated by the actuator, when $w/h > 20$) above the back pressure (generated by the valve), was calculated by assuming a constant flow rate (during valve breakage, an event which took 120 ms). At 3.5 V the micropump produces only an estimated 10 Pa pressure above the stop-valve back pressure, explaining the difficulty in establishing a flow for actuation voltages below 3.5 V. Higher flow rates were observed with increasing voltages.

As expected, the time for the analysis chamber to fill decreased as electrolysis voltage increased (Figure 3a). This is a direct consequence of the rate of gas generation. Regression analysis showed the peak power consumption as a function of voltage was linear between 3.5 and 4.0 V, $r^2 = 0.997$, Figure 3b. Importantly from the point of view of creating a low power device, the peak power consumption at 4 V was more than twice that at 3.5 V (Table 1, Figure 3b). Bubbles generated in the insertion chamber did not recombine quickly after the end of the electrolysis process.[24]

Biosensing. Finally, to show a potential future application for such a device, we integrated a glucose biosensor, based upon the GOD mediated catalytic production of hydrogen peroxide in the presence of oxygen. The enzyme was immobilized within a poly(pyrrole) conducting polymer film, and hydrogen peroxide was detected amperometrically at a potential of 0.85 V versus a pseudo-reference electrode within the analysis chamber. Peak

(24) Pang, C.; Tai, Y. C.; Burdick, J. W.; Andersen, R. A. *Nanotechnology* **2006**, *17*, S64–S68.

oxidation current peaks were found to increase linearly (r^2 = 0.991) with glucose concentration between 1.8 mM and 23.2 mM (Figure 4). In principle, this system could be integrated on-chip, as a remote sensing device, with the calculated sensor sensitivity used in an algorithm within an embedded processor to calculate the glucose concentration of an unknown sample.

CONCLUSION

The paper describes the theory, characterization, and implementation of a valve and its integration with a low power microfluidic pump, based upon gas electrolysis, to move analyte to a biosensor. The low voltages and peak power consumptions, coupled with the small size of the device, demonstrate the potential to create an autonomous embedded biosensing microsystem. This design was compatible with a power supply from a battery, providing a reproducible method for filling a biosensing chamber. Given its size and versatility, this device might also be used as part of a drug delivery mechanism or as a microfluidic insertion within a diagnostic pill platform.

ACKNOWLEDGMENT

This work was jointly funded by the BBSRC and Unilever Ltd. (BBS/S/N/2005/12396). The authors also wish to acknowledge staff of James Watt Nanofabrication Centre of the University of Glasgow for their technical help.

Received for review September 22, 2008. Accepted December 10, 2008.

AC802006D